Assessing the Webb-Pearman-Leuning Formula in Estimating CO_2 Flux at a Tropical Coast

Muhammad Fikri Sigid [1,*], Yusri Yusup [1,2], Abdulghani Essayah Swesi [1], Haitem M Almdhun [1], and Ehsan Jolous Jamshidi [1]

[1] Environmental Technology, School of Industrial Technology, Universiti Sains Malaysia, USM 11800, Pulau Pinang, Malaysia.

[2] Centre for Marine & Coastal Studies (CEMACS), Universiti Sains Malaysia, Pulau Pinang, Malaysia.

Corresponding author: Yusri Yusup (yusriy@usm.my)

Key Points:

- The Webb-Pearman-Leuning formula improves CO_2 flux measurement accuracy in tropical coastal waters using eddy covariance method.
- The Webb-Pearman-Leuning correction produces a lower magnitude flux than the uncorrected CO_2 flux, minimizing the CO_2 flux overestimation.
- The Webb-Pearman-Leuning correction can alter the sign of CO_2 flux, emphasizing the conscientious implementation of the formula.

Abstract

The Webb-Pearman-Leuning (WPL) formula is used to minimize the overestimate CO_2 flux by open-path gas analyzer and eddy covariance methods. However, its effectiveness for tropical coastal waters with high air water vapor content requires investigation. This paper assesses the WPL correction on CO_2 flux measurement over the tropical coastal water using three calculation methods: standard (including WPL and other correction methods), raw, and WPL. The results showed that the standard method yielded CO_2 flux of -0.10 µmol m^{-2} s^{-1}, which is 60% lower than the raw. The WPL-CO_2 flux (-0.07 µmol m^{-2} s^{-1}) is also lower than the raw (-0.25 µmol m^{-2} s^{-1}) by 0.17 µmol m^{-2} s^{-1}. The WPL formula serves its purpose in minimizing the CO_2 flux overestimation but uses caution with the formula as it can change positive-negative flux signs, especially with temperature and water vapor corrections.

Plain Language Summary

The Webb-Pearman-Leuning (WPL) formula is a method used to correct overestimation of CO_2 flux when measuring gas and wind patterns in the air. It has been found to work well in some areas, but we need to investigate how well it works in tropical coastal waters where the air is very humid. This study looked at how well the WPL formula works in three different ways of calculating CO_2 flux: the standard way (which uses WPL and other methods), the raw way (which doesn't use WPL), and the WPL way. The results showed that the standard way gave a CO_2 flux of -0.10 µmol m^{-2} s^{-1}, which is 60% lower than the raw way. The WPL way gave a CO_2 flux of -0.07 µmol m^{-2} s^{-1}, which is lower than the raw way by 0.17 µmol m^{-2} s^{-1}. The WPL formula is good at correcting overestimation, but we need to be careful when using it, especially when correcting for temperature and humidity, because it can change whether the CO_2 flux is positive or negative.

1. Introduction

Carbon dioxide (CO_2) fluxes can be directly estimated using the eddy covariance (EC) technique (Burba et al., 2013). The EC method is often used by ecosystem researchers because it

52 has the advantage of quantifying mass (e.g., CO_2, methane, water, etc.) and energy (sensible and

53 latent heat) exchanges of expansive areas, such as forests, croplands, and oceans (Chien et al.,

54 2018; Heimsch et al., 2021; Lokupitiya et al., 2016; Nakai et al., 2008; Tokoro & Kuwae, 2018).

55

56 The EC method uses the understanding of the behavior of turbulent eddies and utilizes vertical

57 turbulent exchange principles to calculate the flux using the covariance of the high-frequency

58 mixing ratio of CO_2 or moisture and the vertical velocity component of the wind (McGowan et al.,

59 2016; Stull, 1988). High-frequency measurements of wind velocity components are afforded by

60 sonic anemometers, but the measurement of CO_2 or moisture (H_2O) mixing ratio requires fast-

61 response analyzers. The Infrared Gas Analyzers (IRGA) was developed to measure CO_2 or H_2O

62 mixing ratios at high frequencies (e.g., 10 or 20 Hz). At high frequencies, the rapid-response

63 analyzer could capture turbulent exchange and be able to satisfy the EC method requirement (Jones

64 & Smith, 1977).

65

66 The first type of IRGA that measure CO_2 flux on the ocean was the open-path gas analyzer,

67 and research conducted in the last few decades demonstrated the widespread use of the analyzer

68 in air-sea CO_2 flux studies (Yang et al., 2016). However, previous studies have shown that the use

69 of open-path gas analyzer can result in the overestimation of the CO_2 flux due to the effects of

70 water vapor and temperature (Broecker et al., 1986; Edson et al., 2011; Else et al., 2011; Prytherch,

71 Yelland, Pascal, Moat, Skjelvan, & Srokosz, 2010). To minimize the error in the calculated flux,

72 the correction method of the Webb-Pearman-Leuning (WPL) was developed. The WPL

73 formulation was developed to eliminate the effects of air density fluctuations on the molar density

74 of CO_2 that could occur in the open-path systems (Burba et al., 2008; Miller et al., 2010). Webb et

75 al. (1980) proposed the correction by using a formula that considers air density generated by water

76 vapor and latent heat. Variables of temperature, pressure, and molar density were calculated by the

77 formula to produce the corrected CO_2 flux from the gas analyzer.

78

79 On top of the WPL correction, other corrections are applied to the raw CO_2 flux estimated: 1)

80 wind speed measurement offsets and 2) flux spectral corrections. The offset is necessary because

81 wind speed readings from a sonic anemometer can be inaccurate because of the measurement drift

82 (LI-COR, 2021). The spectral corrections are applied to compensate underestimation of fluxes: 1)

83   the low-pass filtering correction for flux losses due to turbulence fluctuation dampening, and 2)

84   the high-pass filtering correction for flux losses caused by long-term turbulent effects due to the

85   finite averaging time of fluxes (LI-COR, 2021). The procedures of low-pass filtering correction

86   are utilized to correct flux spectral properties and describe flux attenuations due to the imperfect

87   instrumental setup (Moncrieff et al., 1997). The process involves estimating the true co-spectra,

88   determining a low-pass transfer function, and applying the function to the estimated true flux co-

89   spectrum so that a high-frequency flux attenuation can be obtained. In addition, the high-frequency

90   spectral correction performs a simple correction formula based on first-order filters and analytical

91   co-spectra formulation for high-frequency spectral losses and flux co-spectra (Horst, 1997;

92   Massman, 2000, 2001; Moncrieff et al., 1997).

93

94   Some researchers reported that the coastal region is a weak carbon source or uptake (Borges

95   et al., 2005). The net CO_2 flux measured in northwestern Taiwan was -1.75 ± 0.98 µmol m^{-2} s^{-1},

96   with the diurnal flux influenced by local wind speed. Similarly, in Todos Santos Bay, Mexico, the

97   CO_2 flux was -1.32 ± 8.94 µmol m^{-2} s^{-1} (Gutiérrez-Loza & Ocampo-Torres, 2016). The CO_2 flux

98   at Bodega Bay, California, was also a weak source, with 0.39 ± 1.84 µmol m^{-2} s^{-1} during the

99   upwelling period and 0.05 ± 0.79 µmol m^{-2} s^{-1} during the relaxation period (Ikawa et al., 2013).

100   Despite their importance, there is still notable uncertainty in how to parameterize these fluxes for

101   global climate models, and more observations are necessary to gain a better understanding of the

102   role of coastal seas in the global carbon cycle (Chien et al., 2018; Doney et al., 2009; Gutiérrez-

103   Loza & Ocampo-Torres, 2016). Additionally, measuring these fluxes using techniques and

104   corrections is challenging because of the high uncertainties introduced during data processing,

105   especially for smaller fluxes (Else et al., 2011; Prytherch, Yelland, Pascal, Moat, Skjelvan, & Neill,

106   2010). Coastal waters can display high variability in CO_2 flux due to various factors, such as water

107   temperature, salinity, and biological activity (Ikawa et al., 2013). Despite this, wind speed plays a

108   critical role in controlling the magnitude of air-sea CO_2 exchanges, and low wind speeds can

109   restrict gas transfer, resulting in reduced CO_2 fluxes in some cases (Aalto et al., 2021). The flux

110   over the coast is low compared to fluxes on land (He et al., 2015; Zhang et al., 2014), and low

111   wind speed over the coast can be one of the reasons that limit gas transfer modulation over coastal

112   waters (Gutiérrez-Loza & Ocampo-Torres, 2016).

113

High-accuracy measurements of CO_2 flux on coastal waters is essential in understanding the global carbon processes and accuracy of future projection studies of carbon sources and sequestration. So, the application of the WPL correction to CO_2 flux measurements over the coastal waters must be investigated. Therefore, the objective of this paper is to assess the WPL correction method on CO_2 flux measurement at a tropical coastal water location.

2.   Materials and Methods

2.1 The EC Dataset

This analysis uses the *in-situ* EC data collected from an automated weather station called the "Muka Head Station" in the Centre for Marine and Coastal Studies of Universiti Sains Malaysia. The station is located on the northwestern part of Penang, Peninsular Malaysia at 5°28′06"N, 100°12′01"E (see Figure 1a).
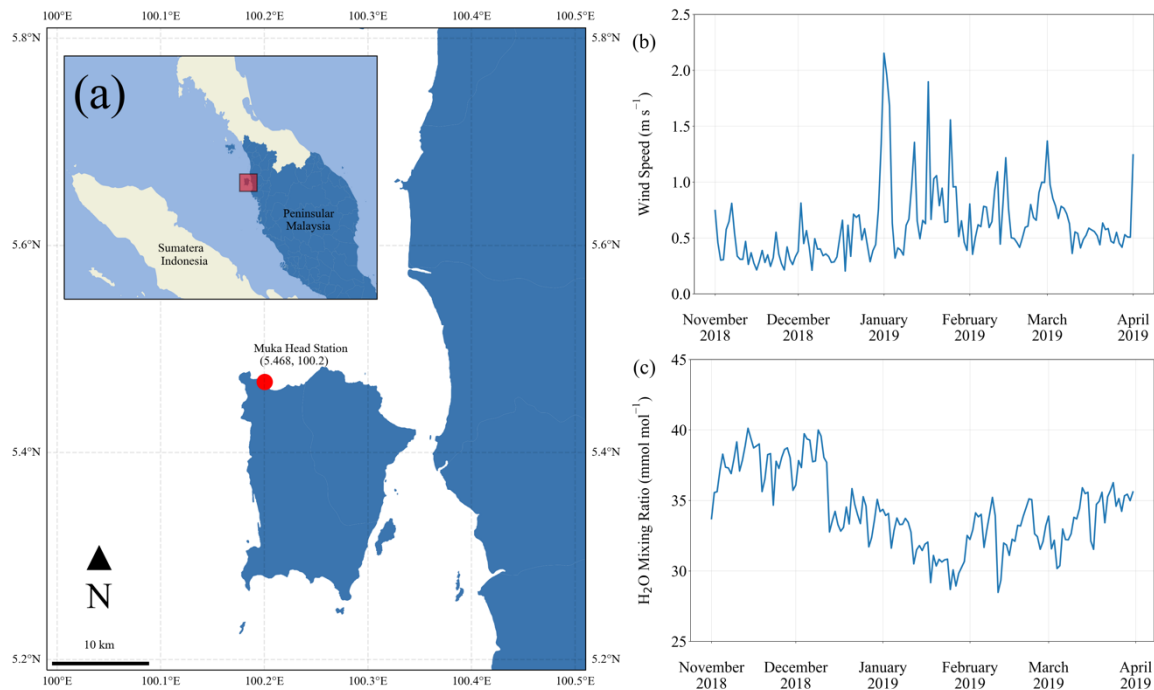

Figure 1 (a) Red circle and box show the location of the automated weather station called the Muka Head Station in Penang, Peninsular Malaysia; (b) the daily-averaged wind speed; (c) the daily-averaged H_2O mixing ratio during the Northeast Monsoon.

Based on Figure 1b, the range of wind speeds in the study location during the Northeast Monsoon is between 0.20 m s^{-1} and 2.15 m s^{-1}, while the average is 0.61 m s^{-1}, which is lower than the coast study area of Gutiérrez-Loza and Ocampo-Torres (2016). Furthermore, the H_2O mixing ratio (refer Figure 1c) has an average of 34.31 mmol mol^{-1}, with a minimum of 28.47 mmol mol^{-1} and a maximum of 40.12 mmol mol^{-1}. Meanwhile, the range of salinity values is relatively low, with a minimum of 32.74 °/oo, a maximum of 34.1 °/oo, and an average of 33.43 °/oo since the site is located over the coast in the tropics, where the salinity is naturally low and does not vary much (Zhu et al., 2009). Overall, the data suggest that there is a relatively low level of salinity and wind speeds.

The station measures CO_2 and H_2O fluxes and bio-meteorological parameters (global radiation, net radiation, seawater temperature, etc.) of a tropical coastal ocean in the Strait of Malacca. The flux is calculated from the 20-Hz data collected by the open-path LI-7500 infrared CO_2/H_2O analyzer (LI-COR, USA) and a sonic anemometer (RM81000, Young, USA). The site is exposed to minimal anthropogenic influence. Other details of the instrumentation can be seen in the published literature (Yusup et al., 2020).

From the entire list of variables available in the dataset, the primary variable analyzed was the EC's CO_2 flux. The data is accessible at http://atmosfera.usm.my and has a time resolution of 30 minutes. The duration of the dataset was from 2015 until 2023, however, the temporal scope of this analysis is five months. The months sampled are in the Northeast Monsoon (November 2018 – March 2019). Analyses and plots were performed and generated using Python ver. 3.9.

2.2 Calculations of the Raw, WPL-Corrected, and Standard CO_2 Fluxes

The CO_2 flux is calculated "raw" using the EC technique. The method applies the vertical turbulence exchange concept to calculate the flux directly by using the vertical wind velocity, molar density of dry air, and the mixing ratio of CO_2 (Aubinet et al., 2000). The EC method uses Equation (1).

$$F_{c,raw} = \overline{\rho_a}\,\overline{w'c'} \qquad (1)$$

163 F_c is CO_2 flux, ρ_a is molar density of dry air, w is vertical component of wind speed, and c is dry

164 air mixing ratio of CO_2.

165

166   The WPL correction method is applied to the raw CO_2 flux calculated using Equation (1). The

167 WPL formula is shown in Equation (2).

168

169 $$F_{c,WPL} = \overline{w'\rho_c'} + (1 + \mu\sigma)\frac{\overline{\rho_c}}{\overline{T}}\overline{w'T'} + \mu\frac{\overline{\rho_c}}{\rho_a}\overline{w'\rho_v'} + (1 + \mu\sigma)\frac{\overline{\rho_c}}{\overline{P}}\overline{w'P'} \qquad (2)$$

170

171 T is temperature, P is pressure, ρ_c is molar density of CO_2, ρ_v is molar density of water vapor, ρ_a

172 is molar density of dry air (Webb et al., 1980). Meanwhile, $\sigma = \rho_v/\rho_a$ and $\mu = M_a/M_v$ with M_a

173 is molecular weight of dry air, M_v is molecular weight of water vapor. The WPL formula consists

174 of the corrections for temperature, water vapor, and pressure fluctuations in the open-path gas

175 analyzer, which are stated in the second, third, and fourth terms in the Equation 2. The first term

176 on the right section of WPL formula is CO_2 flux of EC method that has not been corrected.

177

178   The WPL-corrected CO_2 flux ($F_{c,WPL}$) is compared to the raw CO_2 flux ($F_{c,raw}$) and the

179 standard-calculated CO_2 flux ($F_{c,std}$). $F_{c,std}$ is the CO_2 flux that incorporates other corrections in

180 addition to the WPL correction: 1) wind speed movement offsets, 2) spectral correction of low-

181 pass filtering and high-pass filtering. The methods used to calculate $F_{c,std}$ flux are similar to those

182 utilized in the widely used flux processing software, EddyPro® (ver. 7, LI-COR, USA). In this

183 research, $F_{c,std}$ was used to serve as a benchmark to analyze the application of the WPL correction.

184

185 *2.3 Performance Metrics*

186

187   The comparison among the fluxes calculated involves the correlation among the $F_{c,raw}$, $F_{c,WPL}$,

188 and $F_{c,std}$. This analysis used the Pearson correlation coefficient, which determines the degree of

189 linearity between two quantitative variables and expresses the degree of relationship between

190 them. The coefficient can be positive or negative, depending on the direction of correspondence

191 between changes in the two variables.

192

193   In addition, the evaluation metrics of Root Mean Squared Error (RMSE) and Mean Absolute

194 Error (MAE) were used to measure the magnitude of the error of $F_{c,raw}$ and $F_{c,WPL}$ compared to

195 $F_{c,std}$. The RMSE takes the square root of the average of squared differences to measure the

196 average magnitude of the error, while the MAE calculates the average of the absolute differences

197 between two values to measure the average magnitude of the errors without considering the

198 direction (positive or negative).

199

200 **3.   Results and Discussion**

201

202 *3.1 The $F_{c,std}$ Hourly Cycle at the Tropical Coast*

203

204   Throughout the sampling time domain, $F_{c,std}$ was generally negative, which exhibited that the

205 tropical coast was a CO_2 sink. It is important to note that the sampling domain is in the Northeast

206 Monsoon, which is known to be a period of strong upwelling processes (Gayathri et al., 2022;

207 Mandal et al., 2021; Tan et al., 2006). The magnitude of the negative CO_2 flux varied with the

208 hours (Figure 2a), but it averaged to -0.10 µmol m^{-2} s^{-1}. In the diel cycle, the lowest negative flux

209 occurred during the daytime, with the flux closing to equilibrium at around 14:00 LT. Meanwhile,

210 the CO_2 flux during the nighttime displayed greater uptake movements, with the lowest peak

211 occuring at 06:00 LT.

212

213   This diel cycle is similar to the CO_2 flux trend reported in the Rey–Sánchez et al. (2017) study

214 as carbon uptake, which was conducted at the coastal waters of the Gulf of Aqaba, Israel. Of note

215 is the flux magnitude of this site is lower by 90.48% than the cited study's flux (-1.05 µmol m^{-2}

216 s^{-1}). The similarities can be seen in the trend of negative CO_2 fluxes, which reduced towards

217 equilibrium at 12:00 LT from 06:00 LT; similarly, greater CO_2 uptake occurred during the night.
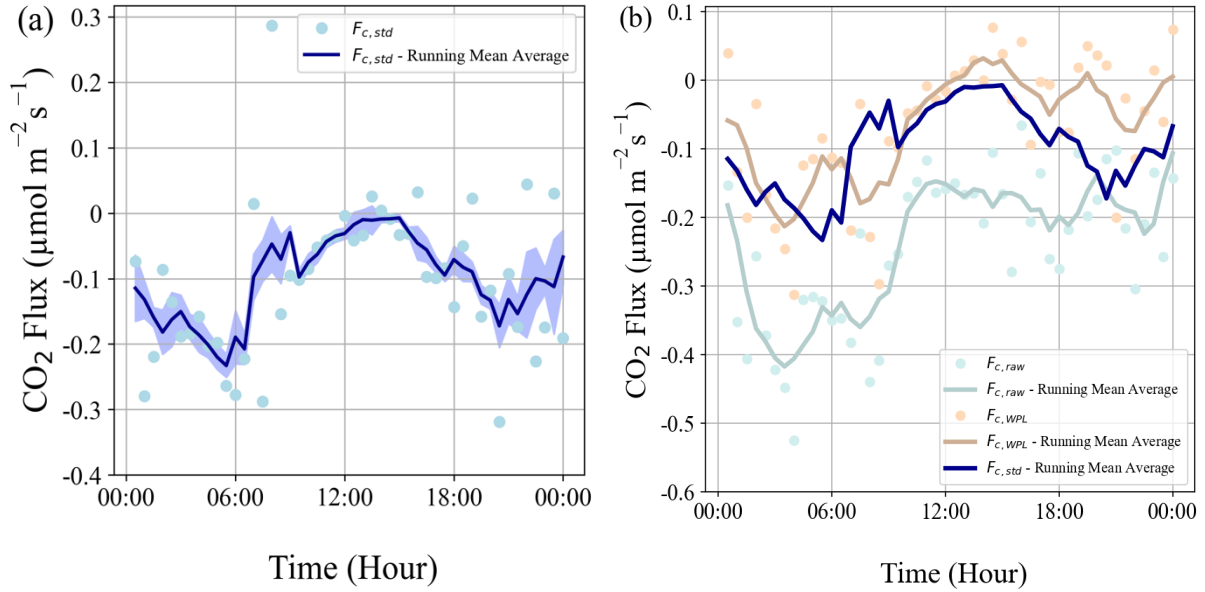
218

Figure 2 (a) The hourly trend of $F_{c,std}$ and its running-mean average at the tropical coast;
(b) the hourly trends of $F_{c,raw}$, $F_{c,WPL}$, and $F_{c,std}$ and their running-mean average.

Figure 2a also displays the standard error of the $F_{c,std}$, indicating a notable level of uncertainty during the morning and evening, but a lower level from 09:00 LT until in the afternoon. On average, the standard error measures 0.02 µmol m^{-2} s^{-1}, ranging from a minimum of 0.005 µmol m^{-2} s^{-1} to a maximum of 0.07 µmol m^{-2} s^{-1}. The observed high uncertainty during specific times may be attributed to fluctuations in evaporation. For instance, an increase in the uncertainty to 0.04 µmol m^{-2} s^{-1} at 08:00 LT was observed due to quite intense fluctuations in evaporation around that time, which may have influenced the CO$_2$ flux's uncertainty.

3.2 Values and Trends Comparison among the $F_{c,raw}$, $F_{c,WPL}$, and $F_{c,std}$

The average values of $F_{c,raw}$ and $F_{c,WPL}$ are –0.25 and –0.07 µmol m^{-2} s^{-1}, respectively, and both display negative fluxes (refer Figure 2b), which is the same as $F_{c,std}$. The decrease of these three fluxes typically was observed between 06:00 LT and 12:00 LT. The lower flux magnitudes can be attributed to the decrease in wind speed during this period, which lowers the transfer velocity and reduces CO$_2$ flux in accordance with the bulk formula (Wanninkhof, 1992; Wanninkhof et al., 2009).

239   There is a varying trend between $F_{c,raw}$ and $F_{c,WPL}$ with $F_{c,std}$. $F_{c,raw}$ and $F_{c,WPL}$ show a

240   significant increase after 00:00 LT, while $F_{c,std}$ increases significantly after 12:00 LT, with another

241   increase occurring from 00:00 LT to 06:00 LT following a decrease before 00:00 LT. The CO_2

242   flux diel cycle reported by Rey-Sánchez et al. (2017) is more similar to $F_{c,raw}$ and $F_{c,WPL}$ fluxes

243   than to $F_{c,std}$.

244

245   The average value of $F_{c,std}$ is significantly lower (higher) than the $F_{c,raw}$ ($F_{c,WPL}$) by –60%

246   (+46%). The difference can be due to the application of correction methods in addition to the WPL

247   correction. According to LI-COR (2021), wind speed measurement offsets and spectral

248   corrections, such as low-pass and high-pass filtering, are necessary in estimating CO_2 flux. The

249   absence of these corrections caused the $F_{c,WPL}$ to be lower, on average magnitude, than the $F_{c,std}$.

250

251   Between $F_{c,raw}$ and $F_{c,WPL}$, $F_{c,WPL}$ is lower than $F_{c,raw}$ by 0.17 µmol m^{-2} s^{-1}. This result is the

252   same as the observation on the open sea by Kondo and Tsukamoto (2007), albeit the magnitude

253   difference in this research is not as significant as theirs. For instance, the magnitude difference by

254   the WPL correction in the cited study is higher by 1.40 µmol m^{-2} s^{-1}. The large difference in the

255   latter study was accompanied by a higher average magnitude of the $F_{c,raw}$ reaching up to 1.42

256   µmol m^{-2} s^{-1}, which can be due to the location of their study, i.e., the open sea with strong winds.

257   On average, the $F_{c,WPL}$ is much lower than the $F_{c,raw}$ flux by >70%–98% for both over the sea and

258   the coastal waters, but it will result in a CO_2 flux value being close to the $F_{c,std}$ as well as CO_2 flux

259   calculated using the bulk transfer equation as measured in Kondo and Tsukamoto (2007). Thus,

260   despite the deviation, the WPL correction still serves its purpose in reducing the overestimation of

261   CO_2 flux collected by the open-path gas analyzers.

262

263   The resulting correlations also highlights the difference in CO_2 flux after applying the WPL

264   correction (see Figure 3). It shows that the correlation of the $F_{c,std}$ and $F_{c,raw}$ (refer Figure 3a) as

265   well as the correlation of the $F_{c,std}$ and $F_{c,WPL}$ (refer Figure 3b) are strong and similar. The

266   correlation between $F_{c,WPL}$ and $F_{c,std}$ is slightly lower than the correlation between $F_{c,raw}$ and

267   $F_{c,std}$, i.e., 0.75 and 0.76, respectively. Moreover, the CO_2 flux trend between the $F_{c,raw}$ and $F_{c,WPL}$

268   is somewhat the same with a very strong correlation ($r = 0.96$) as shown in Figure 3c. It must be

269   pointed out that the lower correlation level between $F_{c,WPL}$ and $F_{c,std}$ does not indicate that the

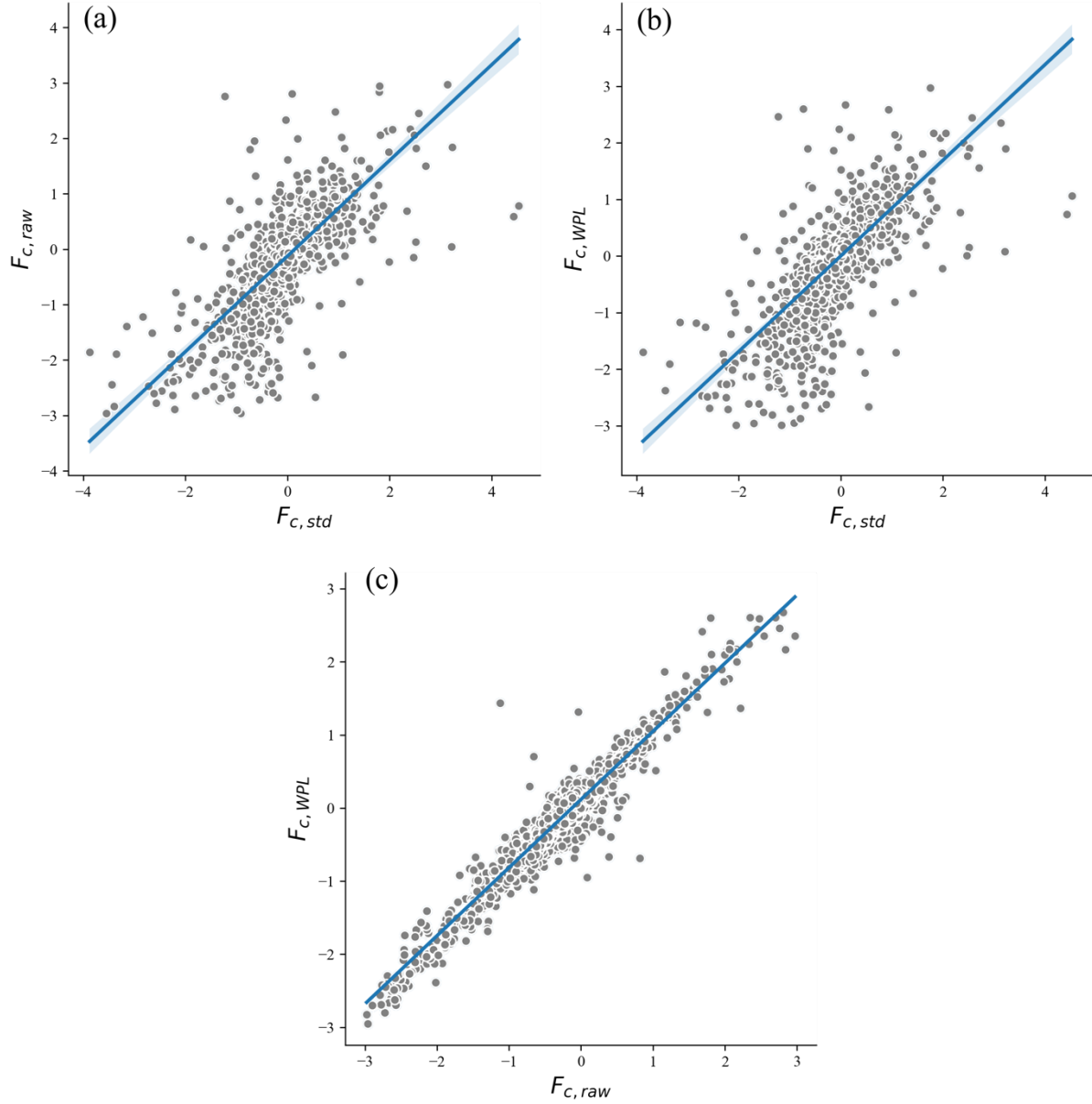270   WPL correction reduces the accuracy of the CO_2 flux estimation.

271

273

274   **Figure 3** The scatter plots for (a) $F_{c,raw}$ and $F_{c,std}$, (b) $F_{c,WPL}$ and $F_{c,std}$, and (c) $F_{c,raw}$ and $F_{c,WPL}$.

275

276   The RMSE values for $F_{c,raw}$ and $F_{c,WPL}$ were found to be 0.35 μmol m^{-2} s^{-1} and 0.33 μmol

277   m^{-2} s^{-1}, respectively, in comparison to $F_{c,std}$. This suggests that the WPL correction reduces the

278   overall error magnitude, resulting in a more accurate estimation of the CO_2 flux. Moreover, the

279   MAE for $F_{c,WPL}$ (0.18 µmol m^{-2} s^{-1}) is also lower than the MAE for $F_{c,raw}$ (0.20 µmol m^{-2} s^{-1})

280   when compared to $F_{c,std}$. This implies that the WPL correction not only reduces the overall error

281   magnitude but also improves the accuracy of the estimated CO_2 flux.

282

283   Nevertheless, the WPL correction also produced positive CO_2 flux several times in the

284   afternoon and the evening, whereas the $F_{c,raw}$ only showed negative fluxes as shown in Figure 2b.

285   For instance, a sign change occurred at 13:30 LT with an $F_{c,raw}$ value of –0.16 µmol m^{-2} s^{-1} and

286   an $F_{c,WPL}$ value of 0.03 µmol m^{-2} s^{-1}. At 16:00 LT, there was also a sign change as the $F_{c,raw}$ value

287   is –0.11 µmol m^{-2} s^{-1} but the $F_{c,WPL}$ value is 0.02 µmol m^{-2} s^{-1}. The different results, particularly

288   in the change of the negative sign to the positive sign of the CO_2 flux, can drastically change the

289   conclusion of the carbon exchange in the studied location. Thus, the WPL correction needs to be

290   implemented conscientiously to achieve a more meaningful CO_2 flux measurement.

291

292   *3.3 Positive-Negative Sign Change of the CO_2 Flux Due to WPL Correction*

293

294   Based on $F_{c,std}$, the tropical coast acted as CO_2 uptake, particularly in January 2019. The $F_{c,std}$

295   has an average of –0.10 µmol m^{-2} s^{-1}, with a similar range of magnitude throughout the Northeast

296   Monsoon; note that the Northeast Monsoon transpire between November and March, annually.

297   The magnitude of $F_{c,std}$ in January also increased in the afternoon, which is the same as the $F_{c,std}$

298   in other months in the Northeast Monsoon.

299

300   Compared to the CO_2 flux diel cycle in the Northeast Monsoon, the flux in January exhibited

301   a different characteristic than the other months of the monsoon (refer Figure 4). The difference is

302   apparent in the magnitude of the $F_{c,std}$ in January; it started to decrease again before 00:00 LT

303   unlike in other months (see section 3.1). Subsequently, the flux in January fluctuated close to

304   equilibrium longer until after 15:00 LT. The difference in the characteristics of the CO_2 flux in

305   January can be interpreted as the monthly variability of meteorological and oceanographic

306   parameters that caused different CO_2 flux responses.

307

308　　　　Based on the CO_2 flux in January (refer Figure 4), the $F_{c,WPL}$ is also lower than the $F_{c,raw}$,

309　　confirming the same results of applying the WPL formula in terms of underestimation. The

310　　absolute average value of the $F_{c,WPL}$ in this month is lower than the $F_{c,raw}$ by 93%. Meanwhile,

311　　the $F_{c,std}$ is lower than the $F_{c,raw}$ by 47% but higher than the absolute $F_{c,WPL}$ by a factor of 75.

312　　The spectral correction methods of the low-pass and high-pass filtering corrections implemented

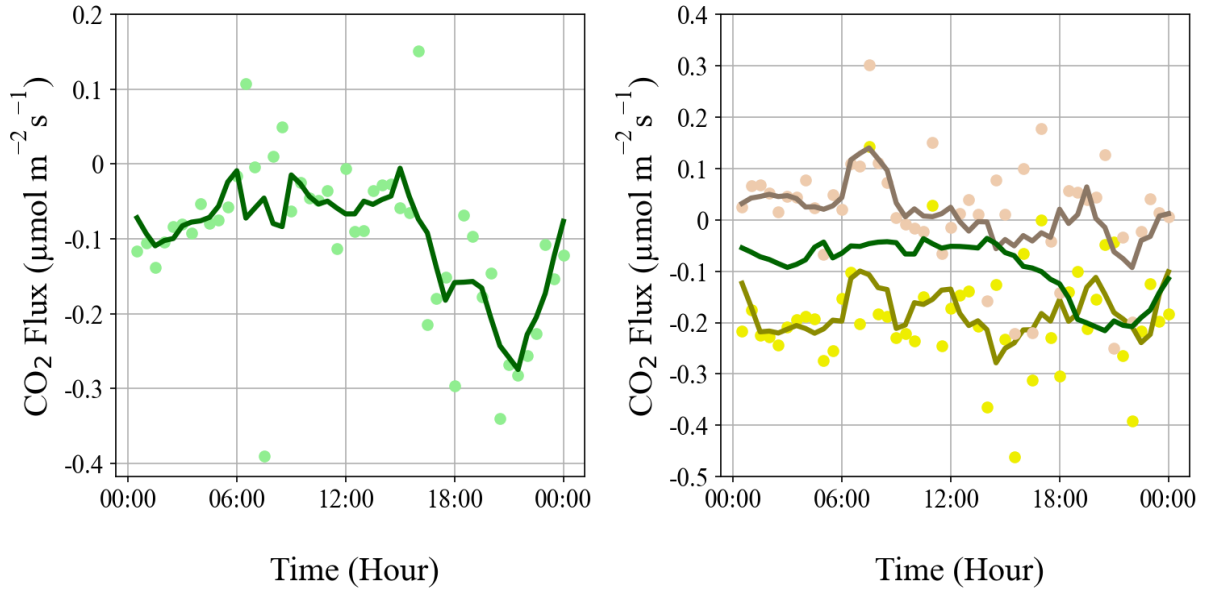313　　in the $F_{c,std}$ appears to prevent the underestimation from resulting a sign change of the flux.

314

315

Figure 4 The hourly trend CO_2 flux for $F_{c,std}$ (left panel) as well as $F_{c,raw}$ and $F_{c,WPL}$ (right

panel) in January 2019. The yellow, brown, and green colors represent $F_{c,raw}$ and $F_{c,WPL}$, and

$F_{c,std}$, respectively. The line is the hourly averaged trend of each $F_{c,raw}$ and $F_{c,WPL}$, and $F_{c,std}$.

319

320　　　　Between $F_{c,raw}$ and $F_{c,WPL}$, the CO_2 flux calculated using the WPL formula displays a pattern

321　　that more closely resembled the $F_{c,std}$. The $F_{c,WPL}$ pattern showed a greater magnitude flux during

322　　evening and lower magnitude flux in the morning until afternoon.

323

324　　　　More importantly, the flux underestimation caused by the WPL formula resulted in a changing

325　　positive-negative sign of the average CO_2 flux. The average for $F_{c,raw}$ is –0.19 µmol m^{-2} s^{-1},

326　　whereas the average for the $F_{c,WPL}$ flux is 0.014 µmol m^{-2} s^{-1}. Compared to the Northeast

327　　Monsoon, the average value of $F_{c,raw}$ in January is lower, which suggests that the likelihood of a

328   sign change increases when the CO_2 flux is lower or closer to equilibrium. Moreover, Figure 4

329   shows there are more positive CO_2 flux from 00:00 LT to 12:00 LT for $F_{c,WPL}$. Hence, the WPL

330   correction causes the negative average value of the $F_{c,raw}$ to change to a positive average value,

331   which indicate the change in the role of the coast as a source or sink of CO_2.

332

333   The WPL correction formula indicates that the measurement of $F_{c,raw}$ is higher in value and

334   should be corrected for temperature, water vapor, and pressure fluctuations. The largest correction

335   values are attributed to temperature and water vapor fluctuations, which averaged to 10^{-6} and 10^{-4}

336      $\mu mol\ m^{-2}\ s^{-1}$, respectively. In contrast, the correction for pressure fluctuations has the least

337   significant effect, the difference in average values is a factor of 10^{300}. Consequently, temperature

338   and water vapor corrections are the most influential factors in altering the sign of CO_2 flux when

339   applying the WPL correction.

340

341   **4   Conclusions**

342

343   The WPL formula was introduced to improve the accuracy of CO_2 flux measurement using

344   the EC method. In this research, the WPL correction was applied on the CO_2 flux measured over

345   the tropical coastal waters to compare the performance of the correction. Three flux calculation

346   methods were evaluated: 1) standard (including WPL and other correction methods), 2) raw, and

347   3) WPL. The $F_{c,std}$ is lower than $F_{c,raw}$ by 60% but is higher than $F_{c,WPL}$ by 46%, which can be

348   due to additional corrections applied to $F_{c,std}$. The $F_{c,WPL}$ ($-0.07\ \mu mol\ m^{-2}\ s^{-1}$) is lower than $F_{c,raw}$

349   ($-0.25\ \mu mol\ m^{-2}\ s^{-1}$) by an average of $0.17\ \mu mol\ m^{-2}\ s^{-1}$. The WPL correction and the standard

350   method produced a clearer hourly CO_2 flux trend than the raw calculated flux. Overall, the WPL

351   formula produces a lower magnitude flux than the uncorrected CO_2 flux by over 70%, serving its

352   purpose in minimizing the CO_2 flux overestimation. However, the temperature and water vapor

353   fluctuations terms in the WPL correction have the greatest impact on altering the positive-negative

354   sign of CO_2 flux. Therefore, the WPL correction needs to be implemented conscientiously to

355   obtain a more accurate CO_2 flux using the EC technique over the tropical coast. Further research

356   is needed to quantify the uncertainty associated with the sign change.

357

358

Open Research

The data used in the study was obtained from the Muka Head Station in the Centre for Marine and Coastal Studies of Universiti Sains Malaysia, it and can be accessed at http://atmosfera.usm.my/api.html (Yusup & Sigid, 2023). The maps used in the study were created through Cartopy version 0.19.0 (Elson et al., 2021), which is a library for creating maps and geospatial data visualizations. Cartopy can be accessed at https://scitools.org.uk/cartopy/docs/latest/. The figures were created using Matplotlib version 3.5.1 (Caswell et al., 2021; Hunter, 2007), which is a tool for creating graphs and plots. Matplotlib is available under the Matplotlib license at https://matplotlib.org/.

References

Aalto, N. J., Campbell, K., Eilertsen, H. C., & Bernstein, H. C. (2021). Drivers of Atmosphere-Ocean CO2 Flux in Northern Norwegian Fjords. *Frontiers in Marine Science*, *8*. https://doi.org/10.3389/fmars.2021.692093

Aubinet, M., Grelle, A., Ibrom, A., Rannik, Ü., Moncrieff, J., Foken, T., Kowalski, A. S., Martin, P. H., Berbigier, P., Bernhofer, Ch., Clement, R., Elbers, J., Granier, A., Grünwald, T., Morgenstern, K., Pilegaard, K., Rebmann, C., Snijders, W., Valentini, R., & Vesala, T. (2000). *Estimates of the Annual Net Carbon and Water Exchange of Forests: The EUROFLUX Methodology*.

388 Borges, A. v., Delille, B., & Frankignoulle, M. (2005). Budgeting sinks and sources of CO2 in the

389 coastal ocean: Diversity of ecosystem counts. *Geophysical Research Letters*, *32*(14), 1–4.

390 https://doi.org/10.1029/2005GL023053

391 Broecker, W. S., Ledwell, J. R., Takahashi, T., Weiss, R., Merlivat, L., Memery, L., Peng, T.-H.,

392 Jahne, B., & Munnich, K. O. (1986). Isotopic versus micrometeorologic ocean CO 2 fluxes:

393 A serious conflict . *Journal of Geophysical Research*, *91*(C9), 10517.

394 https://doi.org/10.1029/jc091ic09p10517

395 Burba, G., Madsen, R., & Feese, K. (2013). Eddy covariance method for CO2 emission

396 measurements in CCUS applications: Principles, instrumentation and software. *Energy*

397 *Procedia*, *40*, 329–336. https://doi.org/10.1016/j.egypro.2013.08.038

398 Caswell, T. A., Droettboom, M., Lee, A., Sales De Andrade, E., Hoffmann, T., Hunter, J., Klymak,

399 J., Firing, E., Stansby, D., Varoquaux, N., Hedegaard Nielsen, J., Root, B., May, R., Elson,

400 P., Seppänen, J. K., Dale, D., Lee, J.-J., McDougall, D., Straw, A., … Ivanov, P. (2021).

401 *matplotlib/matplotlib: REL: v3.5.1*. Zenodo. https://doi.org/10.5281/zenodo.5773480

402 Chien, H., Zhong, Y. Z., Yang, K. H., & Cheng, H. Y. (2018). Diurnal variability of CO2 flux at

403 coastal zone of Taiwan based on eddy covariance observation. *Continental Shelf Research*,

404 *162*, 27–38. https://doi.org/10.1016/j.csr.2018.04.006

405 Doney, S. C., Tilbrook, B., Roy, S., Metzl, N., le Quéré, C., Hood, M., Feely, R. A., & Bakker, D.

406 (2009). Surface-ocean CO2 variability and vulnerability. *Deep-Sea Research Part II: Topical*

407 *Studies in Oceanography*, *56*(8–10), 504–511. https://doi.org/10.1016/j.dsr2.2008.12.016

408 Edson, J. B., Fairall, C. W., Bariteau, L., Zappa, C. J., Cifuentes-Lorenzen, A., McGillis, W. R.,

409 Pezoa, S., Hare, J. E., & Helmig, D. (2011). Direct covariance measurement of CO2 gas

410 transfer velocity during the 2008 Southern Ocean Gas Exchange Experiment: Wind speed

411 dependency. *Journal of Geophysical Research: Oceans*, *116*(11).

412 https://doi.org/10.1029/2011JC007022

413 Else, B. G. T., Papakyriakou, T. N., Galley, R. J., Drennan, W. M., Miller, L. A., & Thomas, H.

414 (2011). Wintertime CO2 fluxes in an Arctic polynya using eddy covariance: Evidence for

415 enhanced air-sea gas transfer during ice formation. *Journal of Geophysical Research:*

416 *Oceans*, *116*(9). https://doi.org/10.1029/2010JC006760

417 Elson, P., de Andrade, E. S., Hattersley, R., May, R., Lucas, G., Campbell, E., Dawson, A.,

418 Raynaud, S., scmc72, Little, B., Donkers, K., Blay, B., Killick, P., Wilson, N., Peglar, P.,

lbdreyer, Andrew, Szymaniak, J., Berchet, A., … Bindle, L. (2021). *SciTools/cartopy: v0.19.0*. Zenodo. https://doi.org/10.5281/zenodo.4707961

Gayathri, N. M., Sijinkumar, A. v, Nath, B. N., Sandeep, K., & Wei, K. Y. (2022). A ~ 30 kyr sub-centennial to millennial Indian summer monsoon variability record from the southern Andaman Sea, northeastern Indian Ocean. *Palaeogeography, Palaeoclimatology, Palaeoecology*, *590*, 110865. https://doi.org/https://doi.org/10.1016/j.palaeo.2022.110865

Gutiérrez-Loza, L., & Ocampo-Torres, F. J. (2016). Air-sea CO2 fluxes measured by eddy covariance in a coastal station in Baja California, México. *IOP Conference Series: Earth and Environmental Science*, *35*(1). https://doi.org/10.1088/1755-1315/35/1/012012

He, Y., Yang, J., Zhuang, Q., Harden, J. W., McGuire, A. D., Liu, Y., Wang, G., & Gu, L. (2015). Incorporating microbial dormancy dynamics into soil decomposition models to improve quantification of soil carbon dynamics of northern temperate forests. *Journal of Geophysical Research: Biogeosciences*, *120*(12), 2596–2611. https://doi.org/10.1002/2015JG003130

Heimsch, L., Lohila, A., Tuovinen, J. P., Vekuri, H., Heinonsalo, J., Nevalainen, O., Korkiakoski, M., Liski, J., Laurila, T., & Kulmala, L. (2021). Carbon dioxide fluxes and carbon balance of an agricultural grassland in southern Finland. *Biogeosciences*, *18*(11), 3467–3483. https://doi.org/10.5194/bg-18-3467-2021

Horst, T. W. (1997). *A simple formula for attenuation of eddy fluxes measured with first-order-response scalar sensors*.

Hunter, J. D. (2007). Matplotlib: A 2D Graphics Environment. *Computing in Science & Engineering*, *9*(3), 90–95. https://doi.org/10.1109/MCSE.2007.55

Ikawa, H., Faloona, I., Kochendorfer, J., Paw U, K. T., & Oechel, W. C. (2013). Air-sea exchange of CO2 at a Northern California coastal site along the California Current upwelling system. *Biogeosciences*, *10*(7), 4419–4432. https://doi.org/10.5194/bg-10-4419-2013

Jones, E. P., & Smith, S. D. (1977). A first measurement of sea-air CO 2 flux by eddy correlation . *Journal of Geophysical Research*, *82*(37), 5990–5992. https://doi.org/10.1029/jc082i037p05990

K Webb, B. E., Pearman, G. I., & Leuning, R. (1980). *Correction of flux measurements for density effects due to heat and water vapour transfer* (Vol. 106).

Kondo, F., & Tsukamoto, O. (2007). Air-Sea CO 2 Flux by Eddy Covariance Technique in the Equatorial Indian Ocean. In *Journal of Oceanography* (Vol. 63).

LI-COR. (2021). *EddyPro Software Instruction Manual*.

Lokupitiya, E., Denning, A. S., Schaefer, K., Ricciuto, D., Anderson, R., Arain, M. A., Baker, I., Barr, A. G., Chen, G., Chen, J. M., Ciais, P., Cook, D. R., Dietze, M., el Maayar, M., Fischer, M., Grant, R., Hollinger, D., Izaurralde, C., Jain, A., … Xue, Y. (2016). Carbon and energy fluxes in cropland ecosystems: a model-data comparison. *Biogeochemistry*, *129*(1–2), 53–76. https://doi.org/10.1007/s10533-016-0219-3

Mandal, S., Behera, N., Gangopadhyay, A., Susanto, R. D., & Pandey, P. C. (2021). Evidence of a chlorophyll "tongue" in the Malacca Strait from satellite observations. *Journal of Marine Systems*, *223*. https://doi.org/10.1016/j.jmarsys.2021.103610

Massman, W. J. (2000). A simple method for estimating frequency response corrections for eddy covariance systems. In *Agricultural and Forest Meteorology* (Vol. 104).

Massman, W. J. (2001). Reply to comment by Rannik on "A simple method for estimating frequency response corrections for eddy covariance systems." In *Agricultural and Forest Meteorology* (Vol. 107).

McGowan, H. A., MacKellar, M. C., & Gray, M. A. (2016). Direct measurements of air-sea CO2 exchange over a coral reef. *Geophysical Research Letters*, *43*(9), 4602–4608. https://doi.org/10.1002/2016GL068772

Moncrieff, J. B., Massheder, J. M., de Bruin, H., Elbers, J., Friborg, T., Heusinkveld, B., Kabat, P., Scott, S., Soegaard, H., & Verhoef, A. (1997). A system to measure surface fluxes of momentum, sensible heat, water vapour and carbon dioxide. In *Journal of Hydrology ELSEVIER Journal of Hydrology*.

Nakai, Y., Matsuura, Y., Kajimoto, T., Abaimov, A. P., Yamamoto, S., & Zyryanova, O. A. (2008). Eddy covariance CO2 flux above a Gmelin larch forest on continuous permafrost in Central Siberia during a growing season. *Theoretical and Applied Climatology*, *93*(3–4), 133–147. https://doi.org/10.1007/s00704-007-0337-x

Prytherch, J., Yelland, M. J., Pascal, R. W., Moat, B. I., Skjelvan, I., & Neill, C. C. (2010). Direct measurements of the CO2 flux over the ocean: Development of a novel method. *Geophysical Research Letters*, *37*(3). https://doi.org/10.1029/2009GL041482

Prytherch, J., Yelland, M. J., Pascal, R. W., Moat, B. I., Skjelvan, I., & Srokosz, M. A. (2010). Open ocean gas transfer velocity derived from long-term direct measurements of the CO2 flux. *Geophysical Research Letters*, *37*(23). https://doi.org/10.1029/2010GL045597

481   Rey-Sánchez, A. C., Bohrer, G., Morin, T. H., Shlomo, D., Mirfenderesgi, G., Gildor, H., & Genin,

482   A. (2017). Evaporation and CO2 fluxes in a coastal reef: an eddy covariance approach.

483   *Ecosystem Health and Sustainability*, *3*(10). https://doi.org/10.1080/20964129.2017.1392830

484   Stull, R. B. (1988). *An Introduction to Boundary Layer Meteorology*.

485   https://doi.org/https://doi.org/10.1007/978-94-009-3027-8

486   Tan, J. C. H., Peters, D. M., & Kaufman, P. L. (2006). Recent developments in understanding the

487   pathophysiology of elevated intraocular pressure. *Current Opinion in Ophthalmology*, *17*(2),

488   168–174. https://doi.org/10.1016/j.csr.2005.09.008

489   Tokoro, T., & Kuwae, T. (2018). Improved post-processing of eddy-covariance data to quantify

490   atmosphere-aquatic ecosystem CO2 Exchanges. *Frontiers in Marine Science*, *5*(AUG).

491   https://doi.org/10.3389/fmars.2018.00286

492   Wanninkhof, R. (1992). Relationship Between Wind Speed and Gas Exchange Over the Ocean. In

493   *JOURNAL OF GEOPHYSICAL RESEARCH* (Vol. 97, Issue C5).

494   Wanninkhof, R., Asher, W. E., Ho, D. T., Sweeney, C., & McGillis, W. R. (2009). Advances in

495   quantifying air-sea gas exchange and environmental forcing. In *Annual Review of Marine*

496   *Science* (Vol. 1, pp. 213–244). https://doi.org/10.1146/annurev.marine.010908.163742

497   Webb, E. K., Pearman, G. I., & Leuning, R. (1980). *Correction of flux measurements for density*

498   *effects due to heat and water vapour transfer* (Vol. 106).

499   Yang, M., Prytherch, J., Kozlova, E., Yelland, M. J., Parenkat Mony, D., & Bell, T. G. (2016).

500   Comparison of two closed-path cavity-based spectrometers for measuring air-water CO2 and

501   CH4 fluxes by eddy covariance. *Atmospheric Measurement Techniques*, *9*(11), 5509–5522.

502   https://doi.org/10.5194/amt-9-5509-2016

503   Yusup, Y., Ramli, N. K., Kayode, J. S., Yin, C. S., Hisham, S., Isa, H. M., & Ahmad, M. I. (2020).

504   Atmospheric carbon dioxide and electricity production due to lockdown. *Sustainability*

505   *(Switzerland)*, *12*(22), 1–12. https://doi.org/10.3390/su12229397

506   Yusup, Y., & Sigid, M. F. (2023). *Assessing the Webb-Pearman-Leuning Formula in Estimating*

507   *CO2 Flux at a Tropical Coast*. https://doi.org/10.6084/m9.figshare.22139939.v1

508   Zhang, H. F., Chen, B. Z., van der Laan-Luijkx, I. T., Chen, J., Xu, G., Yan, J. W., Zhou, L. X.,

509   Fukuyama, Y., Tans, P. P., & Peters, W. (2014). Net terrestrial CO2 exchange over China

510   during 2001–2010 estimated with an ensemble data assimilation system for atmospheric CO2.

511   *Journal   of   Geophysical   Research*,   *119*(6),   3500–3515.

512   https://doi.org/10.1002/2013JD021297

513 Zhu, Y., Shang, S., Zhai, W., & Dai, M. (2009). Satellite-derived surface water pCO2 and air-sea

514   CO2 fluxes in the northern South China Sea in summer. *Progress in Natural Science*, *19*(6),

515   775–779. https://doi.org/10.1016/j.pnsc.2008.09.004

516